

Thickness Dependence of Microstructure in Semiconducting Films of an Oligofluorene Derivative

Dean M. DeLongchamp,^{*,†} Mang Mang Ling,[‡] Youngsuk Jung,[†] Daniel A. Fischer,[†]
Mark E. Roberts,[‡] Eric K. Lin,[†] and Zhenan Bao^{*,‡}

Contribution from the Materials Science and Engineering Laboratory, National Institute of Standards and Technology, Gaithersburg, Maryland 20899, and Department of Chemical Engineering, Stanford University, Stanford, California 94305

Received June 30, 2006; E-mail: deand@nist.gov; zbao@stanford.edu

Abstract: The measurement and optimization of microstructure development in organic semiconductor films is valuable because microstructure in many cases critically impacts electronic performance. We demonstrate a general method to measure microstructure thickness dependence in thin films using surface-sensitive near edge X-ray absorbance fine structure (NEXAFS) spectroscopy. The method is applied to an oligofluorene derivative **DDFTTF**, which consists of a fluorene–bithiophene–fluorene core that is end-substituted with linear dodecyl groups. The substrate-relative orientations of the aromatic core and the aliphatic end chains are independently determined, and comparing these orientations to terrace heights from atomic force micrographs proves that the end chains are interdigitated or folded. By measuring microstructure development from 6 to 150 nm, we find that **DDFTTF** exhibits two different preferential microstructures: one with large terraces within which molecules exhibit a strongly vertical orientation, and one with much smaller domains within which molecules exhibit a mildly horizontal orientation. The relative distribution of these two preferential microstructures depends on the distance of the domains from the substrate and the substrate temperature during deposition. The utility of this method is tested using a lamination technique to measure the saturation hole mobility at the top and bottom interface of **DDFTTF** films. We find that local microstructures with greater π orbital alignment in the source-drain plane correlate directly to better local saturation hole mobilities.

Introduction

The microstructure development of organic semiconductor films critically affects their behavior in a variety of applications such as transistors, photovoltaics, and sensors. The best carrier mobility is expected when a semiconductor film is composed of large, optimally oriented, and connected crystals. For many small molecule semiconductors, the microstructure used in devices is formed upon deposition from a vapor, and its growth is influenced by process conditions such as the substrate temperature, the deposition rate of the semiconductor, and the substrate chemistry.^{1–7} Organic semiconductors with new

primary chemical structures can exhibit new grain structures and molecular packing motifs that can critically impact carrier transport,^{8–12} and consequently the measurement and optimization of microstructure growth have become important tools for organic semiconductor development.

Here, we demonstrate a general method to follow microstructure growth in organic semiconductor films using surface-sensitive near edge X-ray absorbance fine structure (NEXAFS) spectroscopy.¹³ The method can be used to study microstructure and order development in almost any pure or composite organic material that is deposited in a bottom-up fashion upon a planar substrate. We apply this method to study the growth of a vapor-deposited oligofluorene derivative **DDFTTF**, which consists of a symmetric fluorene–bithiophene–fluorene core^{14,15} that is end-substituted in α and ω positions with linear dodecyl groups. The **FTTF** core provides a reasonably high field-effect hole

[†] National Institute of Standards and Technology.

[‡] Stanford University.

- (1) Dimitrakopoulos, C. D.; Brown, A. R.; Pomp, A. *J. Appl. Phys.* **1996**, *80*, 2501–2508.
- (2) Katz, H. E.; Lovinger, A. J.; Laquindanum, J. G. *Chem. Mater.* **1998**, *10*, 457.
- (3) Shtein, M.; Mapel, J.; Benziger, J. B.; Forrest, S. R. *Appl. Phys. Lett.* **2002**, *81*, 268–270.
- (4) Knipp, D.; Street, R. A.; Volkel, A.; Ho, J. *J. Appl. Phys.* **2003**, *93*, 347–355.
- (5) Ruiz, R.; Choudhary, D.; Nickel, B.; Toccoli, T.; Chang, K. C.; Mayer, A. C.; Clancy, P.; Blakely, J. M.; Headrick, R. L.; Iannotta, S.; Malliaras, G. G. *Chem. Mater.* **2004**, *16*, 4497–4508.
- (6) Fritz, S. E.; Martin, S. M.; Frisbie, C. D.; Ward, M. D.; Toney, M. F. *J. Am. Chem. Soc.* **2004**, *126*, 4084–4085.
- (7) Yang, H. C.; Shin, T. J.; Ling, M. M.; Cho, K.; Ryu, C. Y.; Bao, Z. N. *J. Am. Chem. Soc.* **2005**, *127*, 11542–11543.
- (8) Anthony, J. E.; Brooks, J. S.; Eaton, D. L.; Parkin, S. R. *J. Am. Chem. Soc.* **2001**, *123*, 9482–9483.

- (9) Payne, M. M.; Parkin, S. R.; Anthony, J. E.; Kuo, C. C.; Jackson, T. N. *J. Am. Chem. Soc.* **2005**, *127*, 4986–4987.
- (10) Meng, H.; Bendikov, M.; Mitchell, G.; Helgeson, R.; Wudl, F.; Bao, Z.; Siegrist, T.; Kloc, C.; Chen, C. H. *Adv. Mater.* **2003**, *15*, 1090.
- (11) Moon, H.; Zeis, R.; Borkent, E. J.; Besnard, C.; Lovinger, A. J.; Siegrist, T.; Kloc, C.; Bao, Z. N. *J. Am. Chem. Soc.* **2004**, *126*, 15322–15323.
- (12) Curtis, M. D.; Cao, J.; Kampf, J. W. *J. Am. Chem. Soc.* **2004**, *126*, 4318–4328.
- (13) Stöhr, J. *NEXAFS Spectroscopy*; Springer-Verlag: Berlin, 1992; Vol. 392.
- (14) Meng, H.; Zheng, J.; Lovinger, A. J.; Wang, B. C.; Van Patten, P. G.; Bao, Z. N. *Chem. Mater.* **2003**, *15*, 1778–1787.
- (15) Locklin, J.; Li, D. W.; Mannsfeld, S. C. B.; Borkent, E. J.; Meng, H.; Advincula, R.; Bao, Z. *Chem. Mater.* **2005**, *17*, 3366–3374.

mobility and may be more oxidatively stable than a pure oligothiophene core due to its lower HOMO level.¹⁴ The assembly of these cores into well-packed domains may be facilitated by the synthetic addition of long alkyl chains to the 7-position of the two fluorenes, providing a primary chemical structure similar to that of the widely studied α,ω -dihexylsexithiophene.

The **DDFTTF** microstructure was evaluated atop films of increasing thickness to create “growth profiles”, smooth curves that describe the development of molecular orientation within a film as it grows, at three substrate temperatures. The **DDFTTF** molecule exhibits two differently oriented microstructures with a relative distribution that depends on the distance of the domains from the substrate and the substrate temperature during deposition. To test the utility of this growth profile method, a lamination method was used to create double-gated organic field effect transistors (OFETs) that can use either the top or the bottom interface of a semiconducting layer.¹⁶ We find that the local microstructures indicated by the growth profile method correlate directly to different local saturation hole mobilities in the measured regions of the thin semiconductor film.

Experimental Section

The synthesis and purification of oligofluorene derivatives similar to **DDFTTF** have been described previously.^{14,15} **DDFTTF** was synthesized using the Suzuki coupling reaction between 5,5'-dibromo-2,2'-bithiophene and 2-dodecyl-9H-fluorene pinacolato boronic ester. The boronic ester was synthesized via direct cross-coupling between the 2-dodecyl bromofluorene and bis(pinacolato)diboron (Miyaura borylation). The resulting oligomers were purified by repeated washing with hot chloroform followed by vacuum sublimation to yield bright yellow powders. Highly doped n^{++} silicon wafers with thermally grown silicon dioxide (300 nm, capacitance $C_i = 10$ nF/cm²) were cleaned by rinsing with acetone followed by isopropyl alcohol. HMDS surfaces were formed atop these SiO₂/Si substrates using a standard industrial yield enhancement oven (YES brand, model YES-100). **DDFTTF** layers of varying thicknesses were subsequently deposited at a pressure less than 2×10^{-6} Torr with a deposition rate of 0.5 Å/s.

NEXAFS spectroscopy was performed at the NIST/Dow soft X-ray materials characterization facility at the National Synchrotron Light Source (NSLS) of Brookhaven National Laboratory. Carbon K-edge partial electron yield (PEY) spectra were collected at a grid bias of -50 V for a surface-weighted sampling depth of ~6 nm.¹⁷ For PEY spectra, the experimental standard uncertainty of the incident energy is ± 0.15 eV, and the yield uncertainty is $\pm 2\%$.

Carbon K-edge NEXAFS spectra were collected for five to seven incident angles, Θ , from 20° to 70°. Voigt peaks were fit to the $1s \rightarrow \pi^*$ resonance of the conjugated core at 285.4 eV for each of these spectra, and the peak areas were fit to a trigonometric relationship for azimuthally averaged surface-relative orientation of the resonances (essentially a linear fit of peak area vs $\cos^2 \Theta$).¹³ Actual fits were nonlinear to a dichroic ratio, R , which was defined in previous work.¹⁸ The R value can be related to the orientation angle of a vector resonance if a narrow orientation distribution is assumed. Preferential orientation judgments are made with respect to the condition $R = 0$, which corresponds to either a randomly oriented vector orbital or a vector orbital oriented at the “magic angle” of 54.7° from surface normal. If a vector orbital is oriented less than 54.7° away from surface normal, then $R < 0$; if it is a π^* orbital, its conjugated plane is preferentially

flat; and if it is a σ^* orbital, it is preferentially vertical. If a vector orbital is oriented more than 54.7° away from surface normal, then $R > 0$; if it is a π^* orbital, its conjugated plane is preferentially edge on; and if it is a σ^* orbital, it is preferentially horizontal.

Double-gated OFETs were prepared by first evaporating gold gate electrodes onto an HMDS-treated silicon wafer through a shadow mask. A thin layer of poly(dimethyl siloxane) (PDMS, Dow Corning Sylgard 184) was then spin coated onto the gate electrodes from a solution of 20% by weight PDMS in trichloroethylene. A 1:10 wt/wt ratio of cross linker to base was used for the PDMS. The capacitance of the cured PDMS dielectric layer was measured to be 2.9 nF/cm² using an HP 4275A.¹⁶ Gold drain and source electrodes were deposited after curing through a shadow mask to define a channel width of 2 mm and channel length of 100 μ m. To complete the double-gated OFET fabrication, the PDMS assembly with gate electrode, dielectric layer, and source/drain electrodes was laminated atop a **DDFTTF** film that had been evaporated onto HMDS-treated SiO₂ (300 nm) on N-doped silicon (which acts as a second gate). Electrical characterization was carried out using a Keithley 4200SCS semiconductor parameter analyzer, during which the unused gate was always grounded.

NEXAFS Spectra of **DDFTTF**

Peak Assignment. The NEXAFS technique is element-specific by incident energy selection of an absorption edge and bond-specific by the energies and shapes of the resonances detected as absorbance peaks in a spectrum. For an organic semiconductor such as **DDFTTF**, with a structure depicted in Figure 1, the carbon K-edge NEXAFS spectra are rich with features that describe its chemical composition. Labeled spectra of **DDFTTF** are shown in Figures 2a and 3a. The most prominent peak appears at 285.4 eV; this peak arises from the $1s \rightarrow \pi^*$ resonance of the aromatic core. A second peak appears at 287.7 eV, which we attribute to overlapped $1s \rightarrow \sigma^*$ transitions of carbon–hydrogen and carbon–sulfur bonds. The ionization edge occurs at ~290 eV, creating a shoulder. At energies above the ionization edge, the $1s \rightarrow \sigma^*$ transitions of carbon–carbon bonds appear as asymmetric Gaussian peaks, the most prominent being the $1s \rightarrow \sigma_1^*$ peak at 291–293 eV.

The NEXAFS spectra shown in Figures 2a and 3a were collected in partial electron yield (PEY) mode at a bias of -50 V. Approximately 70% of this PEY signal originates within the topmost 4 nm of the illuminated region, describing 1–2 molecular layers. For a 6 nm thick film, PEY spectra represent almost the entire film, whereas for a 40 nm thick film, they represent only the top ~15%. By measuring only the surface molecular orientation, it is possible to follow orientation changes as a film grows thicker, under the assumption that there is minimal surface relaxation. The similarity of the spectral features in Figures 2a and 3a confirms that the chemical compositions of all films are identical. Orientation is revealed where peak intensity varies with incident angle. Deposition on room-temperature substrates creates films where the orientation atop a 6 nm thick film is quite different than it is atop a 40 nm thick film, while deposition on 125 °C substrates creates films where orientation is essentially identical atop 6 and 40 nm thick films.

Analysis of the $1s \rightarrow \pi^*$ Resonance. Within the spectra shown in Figures 2a and 3a, variations in peak intensity with incident angle are especially apparent in the $1s \rightarrow \pi^*$ resonance and in the $1s \rightarrow \sigma_1^*$ resonance. The π^* resonance arises only from the conjugated core, whereas the σ^* resonance includes contributions from both the end groups and the conjugated core, as illustrated in Figure 1. The variation with incident angle of the

(16) Ling, M. M.; Bao, Z. N.; Li, D. W. *Appl. Phys. Lett.* **2006**, *88*, 033502.

(17) Genzer, J.; Kramer, E. J.; Fischer, D. A. *J. Appl. Phys.* **2002**, *92*, 7070–7079.

(18) DeLongchamp, D. M.; Lin, E. K.; Fischer, D. A. *Proc. SPIE* **2005**, *5940*, 54–64.

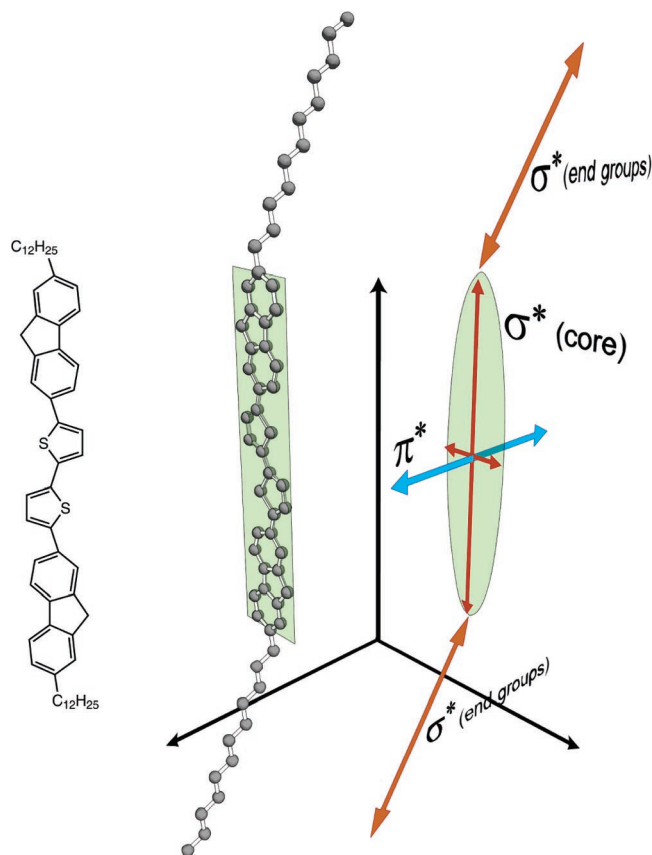


Figure 1. The **DDFTTF** molecule from three perspectives. From left to right: the **DDFTTF** primary chemical structure; an isometric view of **DDFTTF** as optimized by MOPAC (alone in vacuo); a corresponding view of the directionality of **DDFTTF** carbon–carbon vector orbitals in the NEXAFS carbon K-edge. The conjugated plane is represented in green, the σ^* orbital vectors are in orange, and the π^* orbital vector is in blue. The carbon–carbon σ^* of the end groups are considered single vectors parallel to the chain axes.²⁷

$1s \rightarrow \pi^*$ peak intensity describes the substrate-relative orientation of the conjugated plane of the core. The $1s \rightarrow \pi^*$ orientation can be described by a single vector normal to the **FTTF** conjugated plane. The orientation of this vector can be quantified using a dichroic ratio, R , determined by fitting peak areas to the relationship for azimuthally averaged surface-relative orientation, as demonstrated in Figures 2b and 3b.¹⁸

Depositing **DDFTTF** on room-temperature substrates causes its microstructure to comprehensively change as the deposited film grows from 6 to 40 nm thick. Atop the 6 nm thick film, the **DDFTTF** conjugated plane exhibits an R of 0.24, indicating a preference for edge-on orientation (R is defined in Experimental Section). Atop the 40 nm thick film, the conjugated plane exhibits an R of -0.20 , indicating a mild preference for plane-on or flat orientation. Because the PEY collection mode has a sample volume confined to the surface, the change at 40 nm indicates that the topmost material adopts a new microstructure with a new preferential surface-relative orientation. This change may be analogous to the thin-film versus bulk crystalline structures that pentacene crystals exhibit,^{6,19} although for **DDFTTF** the difference is more striking.

Depositing **DDFTTF** on 125 °C substrates results in a homogeneous microstructure throughout the film thickness up to 40 nm. Atop both 6 and 40 nm thick films, the conjugated plane exhibits an R of 0.5, indicating strong edge-on orientation.

An R of 0.5 corresponds to a 73° tilt angle of the conjugated plane normal away from surface normal, if we assume that the orientation distribution is narrow. This deviation from perfect vertical orientation may result from disordered material at grain boundaries, a small population of domains with a different surface-relative orientation, or a slight preferential tilt within the lattice. The terrace formation described in AFM micrographs below leads us to believe that these films are comprehensively ordered with a single packing type, so a slight preferential tilt of the conjugated plane within the lattice is likely.

The observation that higher levels of molecular order can be achieved by depositing **DDFTTF** on a heated substrate is consistent with observations of other small-molecule systems studied by a variety of methods including scanning probe techniques and X-ray diffraction.^{1,3,15,19,20} The effect is generally explained by describing a thermally enhanced two-dimensional surface diffusion that occurs as molecules deposit from vapor. The enhanced molecular motion allows a greater extent of configuration sampling and results in a more equilibrated microstructure and greater domain size.

Analysis of the $1s \rightarrow \pi^*$ Resonance. The $1s \rightarrow \sigma_1^*$ resonance includes contributions from the end group orientation and the core long axis orientation. By considering the manner in which the $1s \rightarrow \sigma_1^*$ peak energy varies with incident angle, it may be possible to deconvolute these contributions. Variation in peak energy can result if different populations of σ^* bonds contribute to NEXAFS spectra collected at different incident angles.

We first consider films deposited on 125 °C substrates, with spectra shown in Figure 3. In these spectra, the $1s \rightarrow \sigma_1^*$ resonance appears at 291.5 eV near normal incidence, whereas it appears at 293.0 eV near glancing incidence. Among bonds formed from the same element, higher energy $1s \rightarrow \sigma^*$ resonances generally indicate shorter σ^* bonds.^{21–23} Single bonds within aromatic ring systems are typically shorter than those within linear aliphatic segments due to strain. Because of this effect, the $1s \rightarrow \sigma_1^*$ resonance appears at 291.0 eV for *n*-hexane,²⁴ 292.2 eV for cyclohexane,²⁵ and 293.1 eV for benzene.²⁶ We conclude that the end chains of **DDFTTF** contribute most to the $1s \rightarrow \sigma_1^*$ resonance near normal incidence, while the core contributes most near glancing incidence. This analysis is predicated on the validity of the building block model, which does not always hold.²⁷ The **DDFTTF** molecule, however, is large and may be treated in the macromolecular sense with the expectation that the orbitals within the core and end subgroups will only weakly interact.

The σ^* orbitals of the conjugated core are oriented primarily along its long axis, as illustrated in Figure 1. The greater $1s \rightarrow \sigma_1^*$

- (19) Ruiz, R.; Mayer, A. C.; Malliaras, G. G.; Nickel, B.; Scoles, G.; Kazimirov, A.; Kim, H.; Headrick, R. L.; Islam, Z. *Appl. Phys. Lett.* **2004**, *85*, 4926–4928.
- (20) Servet, B.; Horowitz, G.; Ries, S.; Lagorsse, O.; Alnot, P.; Yassar, A.; Deloffre, F.; Srivastava, P.; Hajlaoui, R.; Lang, P.; Garnier, F. *Chem. Mater.* **1994**, *6*, 1809–1815.
- (21) Langhoff, P. W.; Rescigno, T. N.; Padiak, N.; Csanak, G.; McKoy, B. V. *J. Chim. Phys. Phys.-Chim. Biol.* **1980**, *77*, 589–598.
- (22) Sette, F.; Stohr, J.; Hitchcock, A. P. *J. Chem. Phys.* **1984**, *81*, 4906–4914.
- (23) Sette, F.; Stohr, J.; Hitchcock, A. P. *Chem. Phys. Lett.* **1984**, *110*, 517–520.
- (24) Hitchcock, A. P.; Ishii, I. *J. Electron Spectrosc. Relat. Phenom.* **1987**, *42*, 11–26.
- (25) Hitchcock, A. P.; Newbury, D. C.; Ishii, I.; Stohr, J.; Horsley, J. A.; Redwing, R. D.; Johnson, A. L.; Sette, F. *J. Chem. Phys.* **1986**, *85*, 4849–4862.
- (26) Hitchcock, A. P.; Fischer, P.; Gedanken, A.; Robin, M. B. *J. Phys. Chem.* **1987**, *91*, 531–540.
- (27) Hahner, G.; Kinzler, M.; Woll, C.; Grunze, M.; Scheller, M. K.; Cederbaum, L. S. *Phys. Rev. Lett.* **1991**, *67*, 851–854.

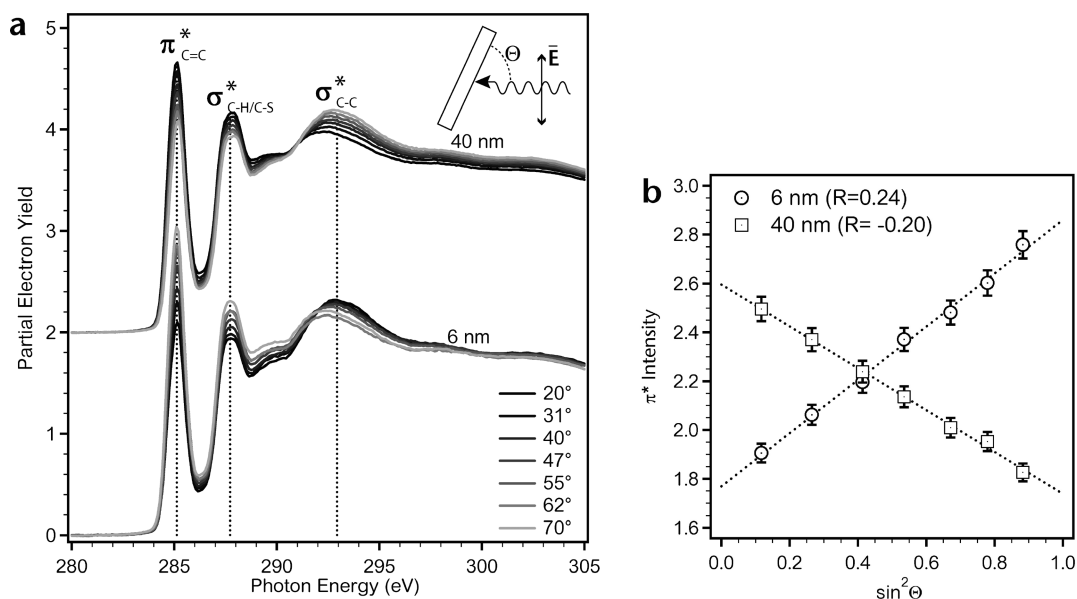


Figure 2. (a) NEXAFS PEY spectra variation with incident angle for films deposited on room-temperature substrates to 6 and 40 nm. (b) Intensity of the π^* resonances in (a) fit to the orientation relationship.

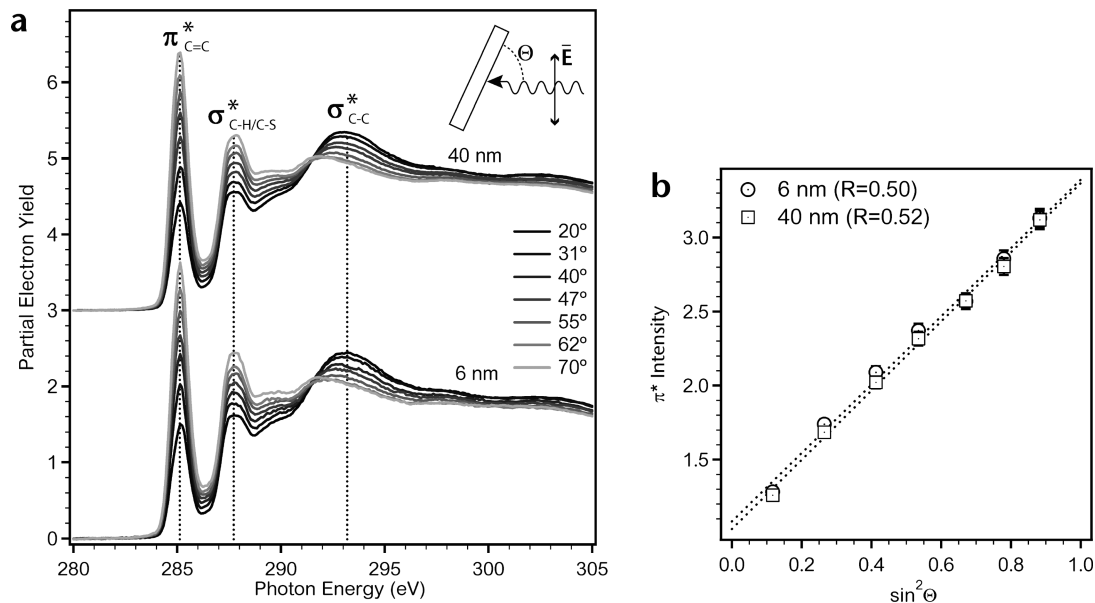


Figure 3. (a) NEXAFS PEY spectra variation with incident angle for films deposited on 125 °C substrates to 6 and 40 nm. (b) Intensity of the π^* resonances in (a) fit to the orientation relationship.

contribution of the core near glancing incidence indicates that the core long axis must be oriented more vertically than the end chains. A vertical core long axis is consistent with the edge-on conjugated plane determined from analysis of the $1s \rightarrow \pi^*$ resonance and is further supported by many reports of an “essentially vertical” orientation of end-substituted oligothiophene cores.^{2,28,29} The angular variation of the entire $1s \rightarrow \sigma_1^*$ resonance indicates a preferentially vertical orientation to the sum of σ^* orbitals ($R \approx -0.23 \pm 0.01$). Because the σ^* orbitals in the end chains considerably outnumber the σ^* orbitals in the conjugated core, the end chains must also be preferentially vertical and tilted less than the “magic” angle of 54.7° away from surface normal; if they were not, the net orientation of the $1s \rightarrow \sigma_1^*$ resonance would be preferentially horizontal.

Because the conjugated core is more vertical than the end chains, the core long axis must be tilted at an even smaller angle.

Identification of Vertical and Horizontal Phases. The combined analysis of the $1s \rightarrow \pi^*$ and $1s \rightarrow \sigma_1^*$ resonances provides a nearly comprehensive picture of **DDFTTF** molecular orientation in films deposited on 125 °C substrates. The cores pack vertically, with a possible slight tilt, whereas the end chains tilt relative to the core. This type of packing has been reported for other symmetrically end-substituted organic semiconductors such as dihexyl sexithiophene. The packing style is rationalized by the different packing densities of the aromatic cores and the aliphatic end chains; the end chains are expected to pack more densely and tilt to adopt the in-plane spacing imposed by the bulkier aromatic cores to which they are covalently attached.³¹

(28) Porzio, W.; Destri, S.; Mascherpa, M.; Bruckner, S. *Acta Polym.* **1993**, *44*, 266–272.

(29) Lovinger, A. J.; Davis, D. D.; Dodabalapur, A.; Katz, H. E. *Chem. Mater.* **1996**, *8*, 2836–2838.

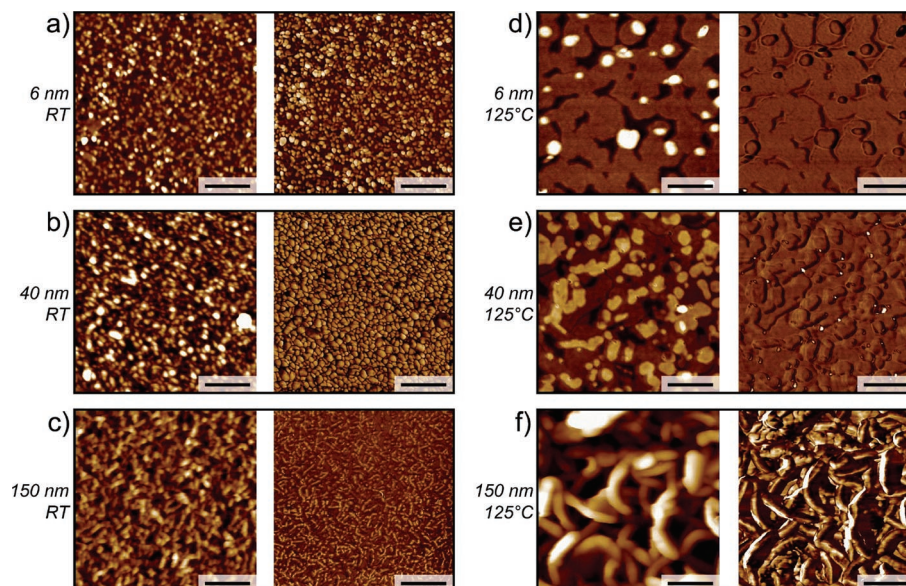


Figure 4. AFM micrographs of **DDFTTF** film topology. Panels are labeled with film thickness and deposition substrate temperature. The scale bar is 500 nm. Height images are presented at left, phase images at right. Height ranges: (a) and (d) are 12 nm; (b) and (e) are 20 nm; (c) is 100 nm; and (f) is 400 nm.

It has been proposed that the molecular-level phase segregation of the end groups away from the cores assists in crystallization, resulting in greater domain sizes for end-functionalized versions of common organic semiconductors.^{2,30–32}

The 40 nm thick film deposited on a room-temperature substrate exhibits a reversal of **DDFTTF** orientation, from an analysis of its $1s \rightarrow \pi^*$ and $1s \rightarrow \sigma_1^*$ intensity trends. The conjugated core appears to pack preferentially flat, rather than edge-on. The core long axis adopts a more horizontal orientation, because the highest energy (shortest) σ^* bonds are observed near normal incidence. The angular variation of the $1s \rightarrow \sigma_1^*$ resonance indicates a preferentially horizontal orientation to the sum of σ^* orbitals ($R \approx 0.14 \pm 0.01$), and the end chains appear to be horizontally oriented as well, but may be less horizontal than the conjugated core. A packing style where the end chains tilt with respect to the conjugated core is again suggested. The absolute values of the core and end chain dichroic ratios are less in this phase than they are in the vertical phase, indicating either fixed orbital orientations closer to 54.7° or some extent of disorder. AFM micrographs, discussed below, suggest that the microstructure is indeed somewhat disordered, with very small domains. This “horizontal phase”, as we will describe it, exhibits a mild preference for horizontal molecular orientation; this description should not be interpreted as a pervasive or absolute horizontal orientation within large domains.

The 6 nm thick film deposited on a room-temperature substrate exhibits an orientation between the strongly vertical orientation and the mild horizontal orientation. A rough quantification of its microstructure composition may be performed based on the R of the conjugated plane. If the film includes regions that are amorphous or randomly oriented ($R = 0$), together with vertically oriented domains ($R = 0.50$), then $\sim 50\%$ is disordered. It is clear, however, that mild horizontal

orientation is possible ($R < -0.20$). If only the vertical and horizontal phases exist within the 6 nm room-temperature film, then 65% would be vertical and 35% would be horizontal. It is likely that some distribution of orientations exists within these ratios.

Correlation of Orientation to Atomic Force Microscopy. Relationships between the nanoscale objects that form in crystal assembly and the packing of the molecules within them can be formed by comparing the molecular orientations observed by NEXAFS spectroscopy to nanometer-scale topographical maps collected by atomic force microscopy (AFM). AFM micrographs were collected for **DDFTTF** films deposited on room temperature and 125 °C substrates; some representative micrographs are shown in Figure 4.

Films of **DDFTTF** deposited on heated substrates exhibit the clearest correlation of orientation to topology. In AFM micrographs of these films, terraces are observed with lateral domain sizes of ~ 400 nm; terrace domains of a particular height appear interconnected and the connection persists for several micrometers. Histogram analysis of these molecular terraces indicates a repeating terrace height of ~ 3.4 nm. Correlation to the NEXAFS orientation analysis would suggest that these terraces are formed by horizontal lamellae of vertically packed cores separated from horizontal lamellae of tilted, packed end chains. A similar packing style has been suggested for aliphatically end-substituted oligothiophenes.^{2,30–32} The conjugated core of **DDFTTF** is ~ 2.4 nm long, while the dodecyl end chains, if all-*trans* and fully extended, would each be ~ 1.6 nm long. If we assume that the core long axes are tilted 17° from surface normal, then the cores contribute ~ 2.3 nm to the AFM terrace height, and by subtraction the tilted end chains contribute ~ 1.1 nm.

Interdigitation or folding of the **DDFTTF** end chains is revealed by comparing the height of the aliphatic portion of the terraces in AFM to the end chain orientation from NEXAFS. From the analysis of the $1s \rightarrow \sigma_1^*$ resonance trend, the maximum allowable end chain tilt away from surface normal is 54.7° (although it is certainly less), which would cause the all-*trans*

(30) Garnier, F.; Yassar, A.; Hajlaoui, R.; Horowitz, G.; Deloffre, F.; Servet, B.; Ries, S.; Alnot, P. *J. Am. Chem. Soc.* **1993**, *115*, 8716–8721.

(31) Katz, H. E. *J. Mater. Chem.* **1997**, *7*, 369–376.

(32) Ackermann, J.; Videlot, C.; Dumas, P.; El Kassmi, A.; Guglielmetti, R.; Safarov, V. *Org. Electron.* **2004**, *5*, 213–222.

dodecyl end chains to extend ~ 1.9 nm vertically (both added together). This vertical height is almost twice their expected ~ 1.1 nm contribution to the terrace height. This comparison proves that end chain interdigitation or folding must occur. We note that specular XRD of **DDFTTF** deposited at 125 °C (presented in Supporting Information) indicates a lamellar out-of-plane packing motif with a slightly larger spacing; our conclusion of end chain interdigitation remains valid for this spacing.

Films of **DDFTTF** deposited on room-temperature substrates exhibit a less clear relationship of orientation to topology. In AFM micrographs collected of 6 and 40 nm thick films, small domains of 50–100 nm in diameter and 3–5 nm in height are observed. Although the average heights of these features are similar to the terrace heights of films deposited on 125 °C substrates, no regular feature height is observed here. In the 6 nm thick film, these domains are associated with a mildly vertical molecular orientation. In the 40 nm thick film, these domains are associated with a mildly horizontal orientation. Because the morphologies revealed by the AFM micrographs are similar for these two thicknesses, we may assume that the same phase is present at both film surfaces. The only explanation for the difference in measured orientation, then, is that one of the films contains a different phase that is buried but still within the sampled volume. It seems most likely that domains of the vertical phase are buried at the substrate interface within the 6 nm film, causing the measured orientation to appear between the vertical and horizontal phases. Specular XRD of films deposited at 25 °C (presented in Supporting Information) indicates that a very small fraction of the lamellar packing motif associated with the vertical phase remains present in thicker films. The Bragg diffraction peak of **DDFTTF** deposited on a 125 °C substrate is ~ 11 times more intense than the peak of **DDFTTF** deposited on a 25 °C substrate. This result is consistent with the determination made by NEXAFS that higher substrate temperature leads to a greater population of a lamellar phase with a vertical molecular orientation, and a greater persistence of this phase as the film grows away from its substrate. There is no clear domain geometry to the horizontal phase. The mild preference for horizontal molecular orientation may be a consequence of small domains with an anisotropic shape, or it could even be an orientation adopted by partially amorphous **DDFTTF**.

Developing Microstructure Growth Profiles

NEXAFS orientation measurements taken in PEY mode are quite surface sensitive. This surface sensitivity allows us to construct a microstructure growth profile, which is a smooth curve that describes the development of microstructure as a semiconductor film grows. Constructing a growth profile may be accomplished by depositing films of many different thicknesses, measuring the orientation at the top interfaces of these films, and then assembling these top layer orientations according to their distance from the substrate. This approach can pinpoint the film thickness at which the orientational aspects of thin film microstructure growth change. We assume that the underlying microstructure foundation remains fixed when additional material is deposited on top of it.

Using the orientation analyses developed above, growth profiles were constructed for **DDFTTF** films deposited on room-

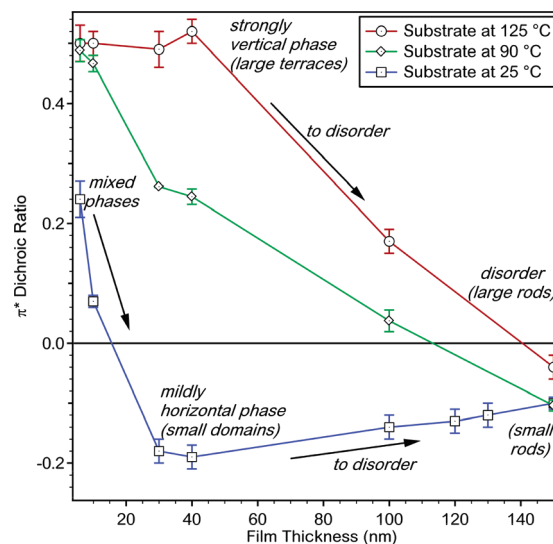


Figure 5. DDFTTF conjugated plane orientation changes with film thickness and substrate temperature.

temperature substrates, 90 °C substrates, and 125 °C substrates. The microstructure is described by the π^* dichroic ratio, R , which indicates the preferred conjugated plane tilt and is correlated to the orientations of the core long axis and the end chains. In Figure 5, growth profiles are presented for film thicknesses ranging from 6 to 150 nm. We observe smooth transitions in microstructure with increasing film thickness, and a monotonic change in the growth profile character with increasing deposition temperature.

The **DDFTTF** films deposited on room-temperature substrates exhibit a change in microstructure close to the substrate, as discussed above. The smooth transition between the 6 and 40 nm dichroic ratios indicates that the relative population of horizontal and vertical phases also shifts smoothly. This smooth shift provides further proof that the 6 nm thick film deposited at room temperature contains mixed phases, with the most vertical phase closest to the substrate. Beyond 40 nm, the orientation remains similar to that of the 40 nm thick film, with a slight trend toward disorder, possibly because the domains lose registration with the substrate plane. AFM micrographs of 150 nm thick films reveal that these domains become small rods that are ~ 200 nm long and ~ 25 nm wide. From the orientation profile, it is clear that **DDFTTF** molecules within these rods are not oriented with the conjugated plane normal parallel to the rod long axis, as has been reported for other organic semiconductors that form rods.^{33–35}

The **DDFTTF** film deposited at 90 °C exhibits more of the vertical phase close to the substrate, and a greater relative population of the vertical phase versus the horizontal phase throughout the film thickness up to 40 nm from the substrate. Between 100 and 150 nm, the orientation appears to trend toward the horizontal phase that was observed over a wide range

- (33) Schenning, A.; Kilbinger, A. F. M.; Biscarini, F.; Cavallini, M.; Cooper, H. J.; Derrick, P. J.; Feast, W. J.; Lazzaroni, R.; Leclere, P.; McDonnell, L. A.; Meijer, E. W.; Meskers, S. C. J. *J. Am. Chem. Soc.* **2002**, *124*, 1269–1275.
- (34) Samori, P.; Francke, V.; Mullen, K.; Rabe, J. P. *Chem.-Eur. J.* **1999**, *5*, 2312–2317.
- (35) Kline, R. J.; McGehee, M. D.; Kadnikova, E. N.; Liu, J. S.; Frechet, J. M. J.; Toney, M. F. *Macromolecules* **2005**, *38*, 3312–3319.

of thicknesses at room temperature. The shift in orientation is remarkably gradual for films deposited on a 90 °C substrate.

DDFTTF deposited on a 125 °C substrate exhibits the greatest persistence of the vertical phase with thickness; the vertical phase is the only phase present up to 40 nm. Beyond 40 nm, the *R* gradually decreases in a manner similar to that of the 90 °C deposited film. At 150 nm from the substrate, the *R* value near zero indicates either a balanced population of horizontal and vertical phases or a random molecular arrangement. AFM micrographs of the surface of this film, shown in Figure 4, reveal a network of large rods with length of 500 nm to 1 μm, width of ~100 nm, and height of several hundred nanometers. It is clear that our thickness measurement of these films (150 nm) is only an average. This surface topology indicates a bulk growth mode; the long axes of the large rods are within the substrate plane only because of their anisotropic shape. From this surface topology, we interpret the zero dichroic ratio of the 150 nm film to indicate substrate-relative disorder of large domains.

This microstructure growth profile method can be generalized to investigate the growth of other organic semiconductors, non-conjugated crystalline or semicrystalline organics, and multilayer self-assembled systems. One limitation is that it requires many films, because the profile quality is determined by the point density. A high-throughput, automated NEXAFS beam line greatly facilitates collection. The controllable surface sensitivity of NEXAFS may make it the most appropriate microstructure analysis tool with which to practice this method. X-ray diffraction, the most powerful alternative tool, does have a controllable sampled volume in grazing incidence mode (GIXD); the sampled volume is controlled by the incident angle, and it is surface sensitive. In GIXD, however, the scattering vector is confined to the substrate plane, and a three-dimensional crystal structure cannot always be solved. Specular diffraction, the out-of-plane complement to GIXD, typically represents an entire sample. The method we describe would be more powerful if NEXAFS were combined with surface-sensitive GIXD, because the complementary molecular orientations and electron density spacings could be compared to quantitatively determine both the extent of crystallinity and the distribution of structures at each film surface.

Correlation to Transistor Data

A principal application of a microstructure growth profile would be to predict the mobility of charge carriers in different regions of a semiconductor film. Most often, organic field effect transistors (OFETs) are bottom-gated, and the field effect mobility is representative of the microstructure at the bottom interface of the semiconductor film. We recently demonstrated a lamination approach to create simultaneously top- and bottom-gated field effect transistors, allowing access to microstructures at both the top and the bottom interfaces of a film.¹⁶ In this approach, a metallized PDMS dielectric is applied to the top interface of the bottom-gated channel of an OFET to act as a second gate. By performing measurements at both interfaces, we can compare saturation hole mobilities within the different **DDFTTF** microstructures that were revealed in the growth profiles.

Top- and bottom-gated transistors were fabricated using **DDFTTF** films that were deposited on room-temperature and

Table 1. Bottom and Top Interface Field Effect Saturation Hole Mobilities for 40 nm Thick **DDFTTF** Films Deposited on a Room-Temperature Substrate and on a 125 °C Substrate

deposition temperature	bottom interface μ_{SAT} ($\text{cm}^2/\text{V}\cdot\text{s}$)	top interface μ_{SAT} ($\text{cm}^2/\text{V}\cdot\text{s}$)
25 °C	1.1×10^{-2}	3.0×10^{-4}
125 °C	1.1×10^{-1}	1.3×10^{-2}

125 °C substrates to ~40 nm thick, with results shown in Table 1. For the film deposited on a 125 °C substrate, the field effect mobility at the bottom interface is greater than that at the top interface by a factor of 10. From the growth profile, the molecular orientations at the bottom and top interface of this film should be similar; in both cases it is vertical. The vertically aligned molecular orientation should be the most advantageous **DDFTTF** microstructure for hole transport because the π -stacking direction is aligned parallel to the source-drain plane. The lower top interface mobility may result from the increased roughness of the carrier plane; a small mobility decrease was also observed in top-gated pentacene films with a rough top surface but a consistently high degree of molecular ordering.¹⁶

The hole mobility from the bottom-gated, room-temperature deposited **DDFTTF** film is lower than that of the film deposited on a 125 °C substrate. The decreased performance is consistent with its growth profile, which indicates that **DDFTTF** molecules at the bottom interface are less vertically oriented than in the film deposited on a 125 °C substrate, which may be a consequence of mixed vertical and amorphous phases or mixed vertical and horizontal phases. The horizontal phase, which appears to be composed of small domains with a mild preferentially horizontal molecular orientation, presumably permits less π -stacking alignment parallel to the source-drain plane, and carrier transfer between molecules within this phase may be less facile. Although comparison with the AFM micrographs did indicate that a buried vertical phase layer might persist at room temperature, these hole mobility measurements suggest that it is not fully continuous or of the same quality as the bottom layer deposited on heated substrates. The horizontal phase exhibits the lowest measured **DDFTTF** mobility in the top-gated 40 nm thick film deposited on a room-temperature substrate. The less optimal π -stacking direction within horizontal phase could be the primary cause of this drop, because the globular domains appear well interconnected in the AFM micrographs and the root-mean-square roughness of the film (4 nm) is not substantially greater than the roughness of the 40 nm film deposited on a 125 °C substrate (3 nm). We note that the globular domains formed on a room-temperature substrate are much smaller than the persistent terraces formed on 125 °C substrates, and the greater number of grain boundaries may also lower the measured hole mobility.

The large variation that we observe in the hole mobility of a single material highlights the importance of microstructure measurement in the analysis and optimization of organic semiconductors. Microstructure growth profiles from NEXAFS spectroscopy can provide a more comprehensive understanding of the complex variations in transport properties that can occur with processing optimization. The structural assignment of

specific chemical moieties, such as the disposition of the aliphatic end chains within the **DDFTTF** microstructure, can illuminate the structural consequences of synthetic strategies, providing molecular design guidelines to lead to new generations of high-performance organic semiconductors.

Acknowledgment. This is an official contribution of the National Institute of Standards and Technology and is not subject

to copyright in the United States. We thank R. J. Kline of NIST for useful discussions concerning AFM technique.

Supporting Information Available: Details of specular X-ray diffraction and OFET transfer curves. This material is available free of charge via the Internet at <http://pubs.acs.org>.

JA064384Q